Changes in the structure of saléeite during dehydration were followed by the use of Raman microscopy in conjunction with a thermal stage. Five stages of dehydration are observed at 43, 73, 87, 231 and 376 °C with the loss of 3, 3, 2, 1 and 1 moles of water.

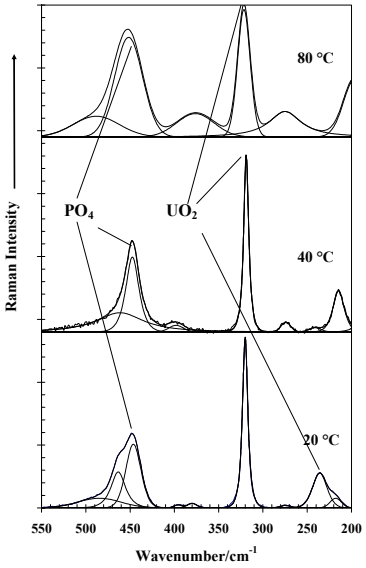

Ray L. Frost and Matt L. Weier

Hot Stage Raman spectroscopic study of the thermal decomposition of saléeite

Hot Stage Raman spectroscopic study of the thermal decomposition of saléeite

Ray L. Frost[•] and Matt L. Weier

Inorganic Materials Research Program, School of Physical and Chemical Sciences, Queensland University of Technology, GPO Box 2434, Brisbane Queensland 4001, Australia.

Published as:
Frost, R.L. and M.L. Weier, Hot-stage Raman spectroscopic study of the thermal decomposition of saleeite. Journal of Raman Spectroscopy, 2004. 35(4): p. 299-307.

Abstract

Hot stage Raman spectroscopy has been used to study the changes in structure of saléeite ($Mg(UO_2)_2(PO_4)_2.10H_2O$) during dehydration. Raman spectra were obtained using a Renishaw Raman microscope coupled with a Linkham thermal stage. Temperatures for Raman spectroscopic analysis were selected by studying the high resolution thermogravimetric analysis of the mineral saléeite. Five stages of dehydration are observed at 43, 73, 87, 231 and 376 °C with the loss of 3, 3, 2, 1 and 1 mole of water respectively. Three antisymmetric PO_4 stretching vibrations are observed at 1007, 994 and 980 cm^{-1}. No symmetric stretching vibration is observed until after significant dehydration has occurred at 75 °C, when a low intensity band at 927 cm^{-1} is observed. Two bands at 843 and 827 cm^{-1} are attributed to the symmetric stretching modes of the two UO_2 vibrational modes resulting from the two non-equivalent UO bonds. The low intensity band at 894 cm^{-1} is assigned to the UO_2 antisymmetric stretching mode. The complexity that is observed in the ν_3 antisymmetric stretching region of the PO_4 units is also observed in the PO_4 ν_2 bending region. Four bands are observed at 471, 446, 405 and 376 cm^{-1}. Two bands observed at 283 and 234 cm^{-1} are assigned to the $(UO_2)^{2+}$ bending modes. After dehydration it is suggested that the structure loses its distortion, takes on a tetragonal structure and hence the Raman spectra become less complex upon thermal treatment.

Keywords: saléeite, autunites, metaautunites dehydration, dehydroxylation, Raman spectroscopy, high-resolution thermogravimetric analysis

Introduction

There are more than 200 uranium minerals; many of which exist in Australian deposits [1]. The chemistry of uranium is important for the solution of environmental problems; for example the remediation of contaminated sites and the restoration of soils such as might be found at Woomera, Australia. One possibility of remediation is

[•] Author to whom correspondence should be addressed (r.frost@qut.edu.au)

through thermal treatment. The use of phosphates media may used as backfill materials in radioactive waste repositories and in the in-situ stabilisation of radioactive nuclides and heavy metals in soils and sediments. Uranyl phosphates and arsenates form one of the largest and most widespread groups of uranium minerals [1]. The minerals are known as autunites and also as the uranyl micas. Many of these minerals may be found in quite widespread parts of Australia [2]. The autunite group of minerals are tetragonal uranyl arsenates, phosphates and vanadates. Of the known 36 or more minerals of the autunite-metaautunite series, only some six minerals have well defined single crystal structures. Of the autunite series, the minerals autunite [3], kahlerite [4,5], novácekite and zeunerite [6] have been determined. Raman spectroscopy allows the possibility of studying the structure at least at the molecular level.

The uranyl mica minerals have a general formula $M(UO_2)_2(XO_4)_2.8\text{-}12H_2O$ where M may be Ba, Ca, Cu, Fe^{2+}, Mg, Mn^{2+} or ½(HAl) and X is As, or P. The minerals are sometimes known as the autunite group of minerals. Autunites are common minerals, yet have been rarely studied in terms of Raman spectroscopy or thermal analysis [7-10]. The minerals have a layer-like structure [9,11,12]. A characteristic feature of the minerals is their layer structure in which uranium is bound in uranyl-phosphate layers. The cations and water are located in the interlayer space. The mineral autunite has the formula $Ca[(UO_2)_2(PO_4)]_2.12(H_2O)$. Autunite is amongst the most abundant and widely distributed of the uranyl phosphate minerals, yet because of its pseudo-tetragonal symmetry and rapid dehydration in air, the details of its symmetry and structure are uncertain. The structure contains the well-known autunite type sheet with composition $[(UO_2)(PO_4)]$, resulting from the sharing of equatorial vertices of the uranyl square bipyramids with the phosphate tetrahedra [13]. The calcium atom in the interlayer is coordinated by seven H_2O groups and two longer distances to uranyl apical O atoms. Two symmetric independent H_2O groups are held in the structure only by hydrogen bonding [11].

Most uranyl minerals are hydrated and as such both water and hydroxyls play a significant role in the structures. It is common for water to play a major role in the degree of polymerisation because of the asymmetric nature of hydrogen bonding systems. Water may bond to the interstitial cation or may simply be held in the structure through hydrogen bonding. Water groups play an important role in satisfying bond-valence requirements. The role of water and the number of water units in the empirical formula determines structural arrangements in the uranyl mica interlayer [1]. For example:

$Ca(UO_2)_2(PO_4)_2.12H_2O$ (autunite) → $Ca(UO_2)_2(PO_4)_2.8H_2O$ (metaautunite I)

$Ca(UO_2)_2(PO_4)_2.8H_2O$ (metaautunite I) → $Ca(UO_2)_2(PO_4)_2.xH_2O$ (metaautunite II).

Burns proposed that uranyl mineral structures be based upon a topological arrangement of anions within each sheet as a convenient basis for the classification of these sheets [14]. The difference between the autunite group and the metautunites is simply the number of water molecules in the formula. The moles of water in the autunites can be variable; whereas the moles of water in metautunite are 8 moles. Zeunerite is the mineral $Cu(UO_2)_2(AsO_4)_2.12H_2O$ and saléeite is the mineral $Mg(UO_2)_2(PO_4)_2.10H_2O$.

Saléeite has been shown to be monoclinic, space group P21/c [15]. The structure consists of UO_2PO_4 sheets, similar to those in threadgoldite, between which are

located Mg^{2+} ions and water molecules. The Mg^{2+} ions are octahedrally coordinated to 6 of the 10 interlayer waters, but the last four waters are not bound to Mg. Saléeite is pseudo tetragonal, the last few water molecules distorting it from true tetragonal symmetry. Previous assignments of saléeite as tetragonal were suggested to be incorrect; the other fully hydrated members of the autunite series may also have symmetry lower than the tetragonal symmetry assumed in the literature. Our interest in minerals with clay-like structures causes our motivation in this research as does the search for fundamental knowledge of minerals containing phosphate and arsenate anions [16-19]. In this work we report the thermal transformation of saléeite a magnesium based uranyl phosphate as studied by hot-stage Raman spectroscopy.

Experimental

Minerals

Saléeite (M20948) was obtained from Museum Victoria and originated from Gilgai, New England, New South Wales, Australia. The mineral was analysed by X-ray diffraction for phase purity and by electron probe for chemical composition.

Thermal Analysis

Thermal decomposition of the saléeite was carried out in a TA® Instruments incorporated high-resolution thermogravimetric analyzer (series Q500) in a flowing nitrogen atmosphere (80 cm^3/min). Approximately 50mg of sample was heated in an open platinum crucible at a rate of 2.0 °C/min up to 500°C. With the quasi-isothermal, quasi-isobaric heating program of the instrument the furnace temperature was regulated precisely to provide a uniform rate of decomposition in the main decomposition stage. The TGA instrument was coupled to a Balzers (Pfeiffer) mass spectrometer for gas analysis. Only selected gases were analyzed.

Hot Stage Raman microprobe spectroscopy

The crystals of saléeite were placed and orientated on the stage of an Olympus BHSM microscope, equipped with 10x and 50x objectives and part of a Renishaw 1000 Raman microscope system, which also includes a monochromator, a filter system and a Charge Coupled Device (CCD). Raman spectra were excited by a HeNe laser (633 nm) at a resolution of 2 cm^{-1} in the range between 100 and 4000 cm^{-1}. Repeated acquisition using the highest magnification was accumulated to improve the signal to noise ratio. Spectra were calibrated using the 520.5 cm^{-1} line of a silicon wafer. In order to ensure that the correct spectra are obtained, the incident excitation radiation was scrambled. Previous studies by the authors provide more details of the experimental technique. Spectra at elevated temperatures were obtained using a Linkam thermal stage (Scientific Instruments Ltd, Waterfield, Surrey, England). Details of the technique have been published by the authors. [20-23] Spectral manipulation such as baseline adjustment, smoothing and normalisation was performed using the GRAMS® software package (Galactic Industries Corporation, Salem, NH, USA).

Results and discussion

High Resolution Thermogravimetric Analysis and Mass spectrometric analysis of saléeite

Saléeite has the formula $Mg(UO_2)_2(PO_4)_2.10H_2O$ and the thermal decomposition is expected to follow a dehydration step-wise process. The thermogravimetric analysis illustrated in Figures 1a and 1b clearly shows these steps. The first step occurs at 41 °C where a weight loss of 5.72% is found. Two weight loss steps which overlap occur at 73 and 87 °C where 5.75 % and 3.8% weight loss occurs. Two further weight loss steps occur at higher temperatures at 231 and 376 °C where 2.0 and 1.5% weight losses are observed. These five weight loss steps are attributed to dehydration. A high temperature weight loss is observed at around 950 °C and is ascribed to the loss of phosphate. The total theoretical weight loss based upon the above formula is 19.3%. The total weight loss determined experimentally is 18.7% in good agreement with the theoretical value. Figure 2 shows the total ion current of water over the temperature range ambient to 500 °C. The total ion current represents the mass spectrum of the evolved water vapour. The temperatures for the total ion current for the evolved water vapour are in excellent agreement with the temperatures shown for the DTG curves.

Stages of the thermal decomposition of saléeite:

The thermal decomposition of saléeite results in the loss of water in five stages with a total weight loss of 18.7%. If the assumption is made that this percentage represents 10 moles of water in the formula, then 1.87 % weight loss represents 1 mole. Hence 5.7% weight loss in the first step represents a loss of three moles of water. Hence the successive stages of the thermal decomposition as proposed below are suggested.

Stage 1

$Mg(UO_2)_2(PO_4)_2.10H_2O \rightarrow Mg(UO_2)_2(PO_4)_2.7H_2O + 3\ H_2O$ 43 °C

Saléeite →metasaléeite I

Stage 2

$Mg(UO_2)_2(PO_4)_2.7H_2O \rightarrow Mg(UO_2)_2(PO_4)_2.4H_2O + 3\ H_2O$ 73 °C

Metasaléeite I → metasaléeite II

Stage 3

$Mg(UO_2)_2(PO_4)_2.4H_2O \rightarrow Mg(UO_2)_2(PO_4)_2.2H_2O + 2\ H_2O$ 87 °C

Metasaléeite II →metasaléeite III

Stage 4

$Mg(UO_2)_2(PO_4)_2.2H_2O \rightarrow Mg(UO_2)_2(PO_4).H_2O + \quad H_2O$ 231 °C

Metasaléeite III → metasaléeite IV

Stage 5

$Mg(UO_2)_2(PO_4)_2.2H_2O \rightarrow Mg(UO_2)_2(PO_4) + \ H_2O$ 376 °C

Metasaléeite IV → anhydrous magnesium uranyl phosphate

Stage 6

$$Mg(UO_2)_2(PO_4)_2 \rightarrow MgU_2O_7 + P_2O_5 \qquad \sim 950\ ^\circ C$$

The loss of three moles of water at 43 °C results in the formation of metasaléeite I with a formula $Mg(UO_2)_2(PO_4)_2.7H_2O$. The interpretation of this first step is open to question because of the loss of water at quite low temperatures. The data for this step depends on factors such as sample amount, humidity, open or closed vessels, and other experimental factors. Further investigation is required for these low temperature water mass loss steps, possibly using CTRA techniques (controlled rate thermal analysis). At 73 °C, three moles of water are lost and this results in the formation of the tetrahydrate $Mg(UO_2)_2(PO_4)_2.4H_2O$ (metasaléeite II). T\In line with the normal terminology this mineral may be termed the metasaléeite II. At 87 °C, two further moles of water are lost resulting in the formation of the dihydrate $Mg(UO_2)_2(PO_4)_2.2H_2O$ which could be termed the metasaléeite III. The final two moles of water are only lost at higher temperatures. Stage 4 occurs at 231 °C and stage 5 at 376 °C. Previous studies have shown that of the ten water molecules in the saléeite structure six are coordinated to the Mg [15]. A further four molecules are involved in the hydration sphere of the Mg and cause the distortion of the saléeite structure from tetragonal to pseudo-tetragonal or monoclinic.

Hot Stage Raman spectroscopy of Saléeite

There has been considerable research in the infrared spectroscopy of the uranyl micas [12,24-29]. However very few studies of the Raman spectroscopy of the uranyl micas have been forthcoming. Certainly there have been no hot stage Raman spectroscopic studies of the uranyl micas. Some studies have been undertaken comparing the theoretically calculated predicted bands with the experimentally determined bands. Nikanovich et al. calculated the vibrational spectrum of calcium uranyl phosphate hexahydrate and compared the calculated results with the experimentally determined values [30]. By using the structural fragment $[(UO_2)_4(PO_4)]^{5+}$ with D_{2d} symmetry, Nikanovich et al. reported band centres for the ν_1 $(UO_2)^{2+}$ (*A1, B2, E*) as 822 (calculated), and observed as 820 weak (IR) and 828 strong (Raman), and for the ν_3 $(UO_2)^{2+}$ (*A1, B2, E*) 919 (calculated) and 913 (IR)). All these types (*A1, B2, E*) were described as accidental vibrational degeneracy caused by the increase of the number of the degrees of freedom for the system of four identical uranyl groups in comparison with one uranyl group [30]. According to Prins et al. existing data in literature make clear that the wavenumber which belongs to ν_1 $(UO_2)^{2+}$ is in most cases found in the region around 850 cm^{-1}, whereas the other stretching wavenumber ν_3 $(UO_2)^{2+}$ has a distinctly higher wavenumber and is situated in a region near 950 cm^{-1} [31,32]. Complications may arise because of the possibility of coupling between vibrations of different uranyl groups in case two or more of these are present in one and the same molecule or chain. This coupling results in splitting of bands in the vibrational spectra. Interactions between the vibrations of different molecules in the same unit cell may cause a further splitting of bands (factor group splitting), e.g. in synthetic metaschoepite possessing 4 distinct uranium atoms in the unit cell results in the following bands 840wsh, 843wsh, 847vs, 866wsh, 867wsh, 870vvs (Raman) and 856vs broad (IR). Another example is $[(UO_2)_2(OH)_2Cl_2(H_2O)_4]$, with two distinct uranium atoms in the unit cell and 847.5S, 850S, 852sh, 855vvw (Raman) and 851mS,sharp, 873sh, 883m (IR). It is apparent

that there have been no recent studies of the vibrational spectroscopy of the uranyl micas and few Raman spectroscopic investigations [33-37]. Further the single crystal structure of the thermally dehydrated saléeite is unknown.

Hydroxyl stretching region

One means of studying the thermal decomposition of saléeite is through the changes in the structure through dehydration of the mineral. The use of Raman spectroscopy in conjunction with a hot stage enables these molecular structural changes to be observed. Figure 3 shows the spectra of the hydroxyl stretching region of saléeite as a function of temperature. The results of the band component analysis of these spectra re reported in Table 1. Four bands are observed in the Raman spectrum at 30 °C of the hydroxyl stretching region at 3615, 3536, 3496 and 3400 cm^{-1} with bandwidths of 18.7, 42.6, 30.4 and 74.4 cm^{-1}. The significance of the four bands rests with the strength of the hydrogen bonds formed between the water molecules and the UO_2 and PO_4 units. The observation of four bands which are attributed to OH symmetric stretching vibrations suggests that at the molecular level four different non-equivalent water molecules are present.

At 40 °C, three bands are observed at 3615, 3533 and 3391 cm^{-1}. The band at 3496 cm^{-1} is no longer observed. This means that simply heating the mineral from 30 to 40 °C has resulted in the loss of one type of water molecule. Such a change in structure fits well with the first stage in the thermal decomposition of saléeite as determined by HR-TG. The autunite group of minerals are renowned for their variable water composition. Such variation depends on the temperature, the atmospheric pressure and the water vapour pressure. Such variables not only effect the composition of the mineral but may also effect the molecular arrangements of the water molecules in the hydration sphere of the Mg cation in the interlayer of the saléeite. At 55 °C, the spectrum is completely different with bands observed at 3614 and 3602 and a broad band at 3400 cm^{-1}. The latter band is very broad. In the 55 °C spectrum the previously observed band at 3533 cm^{-1} is no longer found. At this temperature it is suggested that two types of water molecules exist in the interlayer structure. In the spectrum at 75 °C, three bands are observed in the hydroxyl stretching region at 3614, 3581 and 3376 cm^{-1}. Following the line of reasoning that each band represents the hydroxyl stretching vibration of a water molecule, it means that at 75 °C three types of water exist in the structure. At 100 and 150 °C, only a single band at 3612 cm^{-1} is observed. No intensity remains in the Raman spectrum above 250 °C. The single band at 100 °C represents the water coordinated to the Mg. Significantly high temperatures are required to remove this type of water molecule.

Phosphate stretching region

The Raman spectrum of the 750 to 1050 cm^{-1} region of the thermally treated saléeite is shown in Figure 4. This figure includes the Raman spectra of the stretching region of both the UO_2 and PO_4 units. Infrared spectroscopy combined with theoretical calculations has shown that the UO_2 symmetric stretching region is centred in the 820 to 840 cm^{-1} region [9,12,24,25]. Phosphate vibrations are well known. In aqueous systems, Raman spectra of phosphate oxyanions show a symmetric stretching mode (ν_1) at 938 cm^{-1}, the antisymmetric stretching mode (ν_3) at 1017 cm^{-1}, the symmetric bending mode (ν_2) at 420 cm^{-1} and the ν_4 mode at 567 cm^{-1}. The

pseudomalachite vibrational spectrum consists of ν_1 at 953, ν_2 at 422 and 450 cm^{-1}, ν_3 at 1025 and 1096 and ν_4 at 482, 530, 555 and 615 cm^{-1} [38,39]. Libethenite vibrational modes occur at 960 (ν_1), 445 (ν_2), 1050 (ν_3) and 480, 522, 555, 618 and 637cm^{-1} (ν_4) [38,39].

A set of overlapping bands is observed in the 980 to 1050 cm^{-1} region for each of the uranyl phosphates. These bands are attributed to the ν_3 PO_4 antisymmetric stretching vibrations. In the spectrum at 30 °C, three bands are observed at 1007, 994 and 980 cm^{-1} with bandwidths of 11.8, 12.8 and 13.1 cm^{-1}. It is noted that no PO_4 symmetric stretching vibration is observed in the Raman spectrum, when it would be expected. It is probable that a band should be observed around 935 cm^{-1}. In the structure of the uranyl micas, the four PO_4 stretching vibrations are non-equivalent [3,5]. This means that the in-phase behaviour of the PO_4 stretching vibrations would not be observed and hence no Raman band of any intensity would result. A very low intensity band is observed at 933 cm^{-1} which may be attributed to the PO_4 symmetric stretching vibration. In the 40 °C spectrum bands are observed in similar positions. However at 55 °C significant changes in the spectra are observed. The band at around 1008 cm^{-1} is no longer observed. Two bands at 995 and 977 cm^{-1} with bandwidths of 15.5 and 10.6 cm^{-1} are observed. Further significant intensity is observed at 927 cm^{-1}. This band is very sharp with a bandwidth of 7.0 cm^{-1}. The bands at 995 and 977 cm^{-1} are assigned to the ν_3 PO_4 antisymmetric stretching vibrations and the band at 927 cm^{-1} to the ν_1 symmetric stretching vibration. It I proposed that upon thermally treating the saléeite to 55 °C, with the associated loss of water, increased symmetry of the PO_4 units are observed. At higher temperatures 75, 100 and 150 °C, the spectra in the ν_3 antisymmetric stretching region show little change; however at 250 °C two bands are observed at 1036 and 997 cm^{-1}; no band is observed at 979 cm^{-1}. A broad band is observed at 934 cm^{-1} ascribed to the ν_1 symmetric stretching mode. These Raman spectroscopic observations indicate that the symmetry of the phosphate is reduced upon heating. At 250 °C with the total dehydration of the saléeite, it means that the planar structure of the mineral is lost and that Mg uranyl phosphate is formed.

UO_2 stretching vibrations

Farmer gave the position of the $(UO_2)^{2+}$ bands as ν_1 at 805 cm^{-1} for torbernite and ν_3 as 915 cm^{-1} [40]. The interpretation of this assignment is open to question. Cejka et al. reported the infrared spectrum of sabugalite and suggested that the weak absorption band at 810 cm^{-1} was attributable to the symmetric stretching mode of the $(UO_2)^{2+}$ unit and that the band at 915 cm^{-1} was attributable to the antisymmetric stretching vibration of the $(UO_2)^{2+}$ unit [7]. The ν_2 bands of the $(UO_2)^{2+}$ units were found at 298 and 254 cm^{-1}. Herein lies the difficulty in that both the ν_1 bands of PO_4 and $(UO_2)^{2+}$ is found at the same spectral positions making interpretation by infrared spectroscopy difficult. Raman spectroscopy clearly shows well-resolved bands in the 800 to 840 cm^{-1} region. These bands are assigned to the UO_2 stretching modes. The crystal structure of autunites [3] shows that the two UO bonds are non-equivalent with different bond lengths. It is assumed a similar situation exists for saléeite [15]. Thus the two bands observed at 843 and 827 cm^{-1} are attributed to the symmetric stretching modes of the two UO_2 vibrational modes resulting from the two non-equivalent UO bonds. The low intensity band at 894 cm^{-1} is assigned to the UO_2 antisymmetric stretching mode. A band is observed at 803 cm^{-1}; this band shifts to higher wavenumbers with thermal treatment. However the intensity of the band is lost by 100

°C. It is not known what the band is due to but one possibility is that the band is due to a water librational mode, which is Raman active. It is noted that thermal treatment results in the loss of intensity in the band at 894 cm^{-1}, such that by 55 °C no intensity remains. The width of the bands at 843 and 827 cm-1 appear to decrease in bandwidth up to 100 °C and then increase with further temperature increase.

PO_4 bending region

Farmer reported the bending modes of autunite ν_2 as 472 and 435 cm^{-1}, and ν_4 as 615 and 545 cm^{-1} [40]. The Raman spectra of the 350 to 750 cm^{-1} region of thermally treated saléeite are shown in Figure 5 and the results of the Raman spectroscopic analysis reported in Table 1. Two bands are observed in the 30 °C spectrum at 612 and 573 cm^{-1}. The bands are attributed to the PO_4 ν_4 out-of-plane bending modes. The band at 573 cm^{-1} is lost after 55 °C. An additional low intensity band is observed at 582 cm^{-1} after thermally treating above 55 °C.

The complexity that is observed in the ν_3 antisymmetric stretching region of the PO_4 units is also observed in the PO_4 ν_2 bending region. Four bands are observed at 471, 446, 405 and 376 cm^{-1}. The band at 405 cm^{-1} shows no intensity after 55 °C and the band at 451 cm^{-1} shows no intensity after 75 °C. X-ray crystallography shows that the saléeite structure is a distorted tetragonal structure induced by the presence of water molecules. After dehydration it is suggested that the structure loses its distortion, probably takes on a tetragonal structure and hence the Raman spectra become simpler upon thermal treatment. At 250 °C, only one band is observed at 468 cm^{-1}.

UO_2 bending region

Cejka et al. reported the infrared spectrum of sabugalite and suggested that the ν_2 bands of the $(UO_2)^{2+}$ unit were found at 298 and 254 cm^{-1} [7,9]. Figure 6 shows the low wavenumber region of the thermally treated saléeite. An intense band is observed at 283 cm^{-1} attributed to the ν_2 bending modes of the UO_2 units. The band shows asymmetry above 75 °C and a second band is observed at 265 cm^{-1}. These bands broaden with temperature increase. Three additional bands are observed at 234, 218 and 196 cm^{-1}. The first two bands show no intensity after 150 °C. A low wavenumber band is also observed at around 177 cm^{-1}.

Conclusions

Hot stage Raman spectroscopy has been used to follow the changes in structure during the dehydration of saléeite. Temperatures for the Raman spectroscopic analysis were selected based upon the thermogravimetric analysis of saléeite. The combination of high resolution thermogravimetric analysis coupled to a gas evolution mass spectrometry has been used to study the thermal decomposition of the mineral saléeite ($Mg(UO_2)_2(PO_4)_2.10H_2O$). Five stages of dehydration are observed at 43, 73, 87, 231 and 376 °C. The temperatures of these dehydration steps were then used as the temperatures at which Raman spectra of the thermally decomposed sample were obtained. These Raman spectra were then used to characterise the changes in the molecular structure of the saléeite. Very significant changes in the Raman spectra were obtained at these temperatures. The crystal

structure of saléeite shows that the structure is a distorted tetragonal structure. This distortion was brought about by the hydrogen bonding of the water molecules to the PO_4 and UO_2 units. The loss of water between 40 and 55 °C results in the removal of this distortion resulting in simpler Raman spectra. Further dehydration above 100 °C results in the loss of the layer structure, resulting in increased complexity in the Raman spectra. Dehydration of the mineral is readily followed by the changes in the spectra of the hydroxyl stretching region.

One of the difficulties in assigning the bands of the autunite minerals is the overlap of the stretching vibrations of the UO_2 and PO_4 and/or AsO_4 units. The AsO_4 and UO_2 stretching vibrations occur in almost identical positions. The further complexity is introduced because of the distorted structure of the saléeite unit cell. This results in a reduction in symmetry, with several bands being found in the PO_4 antisymmetric stretching region. In the structure of saléeite the four PO bonds are non-equivalent brought about by the non-equivalence of the two UO_2 bonds. Such non-equivalence results in the lack of intensity of the ν_1 PO_4 stretching band. This band only becomes observed after the initial dehydration steps which results in the removal of the distorted tetragonal structure.

Three antisymmetric stretching vibrations are observed at 1007, 994 and 980 cm^{-1}. No symmetric stretching vibration is observed until after significant dehydration has occurred at 75 °C, when a low intensity band at 927 cm^{-1} is observed. The complexity that is observed in the ν_3 antisymmetric stretching region of the PO_4 units is also observed in the PO_4 ν_2 bending region. Four bands are observed at 471, 446, 405 and 376 cm^{-1}. The loss of degeneracy is removed by dehydration and the four bands become two bands after dehydration suggesting the increased symmetry upon dehydration. It is possible that dehydration causes a displacement of the layers in the saléeite upon thermal treatment.

The structure of saléeite is such that the two UO bonds are non-equivalent. These results in the observation of two UO stretching bands observed at 843 and 827 cm^{-1}. A low intensity band is observed at around 894 cm^{-1} and is attributed to the UO_2 antisymmetric stretching vibration. A complex set of bands is observed in the low wavenumber region. These bands are assigned to the UO_2 bending vibrations. Bands are observed at 283, 234, 218 and 196 cm^{-1} and are all assigned to UO_2 bending modes. The complexity of the UO_2 bending modes is observed up to 250 °C. This complexity is lost only after dehydration.

Acknowledgements

The financial and infra-structure support of the Queensland University of Technology Inorganic Materials Research Program of the School of Physical and Chemical Sciences is gratefully acknowledged. The Australian Research Council (ARC) is thanked for funding. Mr Dermot Henry of Museum Victoria is thanked for the supply of the saléeite minerals. Professor Jiri Cejka of the National Museum, Václavské náměstí 68, CZ-115 79 Prague 1, Czech Republic, is especially thanked for many useful and interesting discussions.

References

1. Burns, P. *Reviews in mineralogy Vol 38* 1999**; 38**: 23.
2. Isobe, H, Ewing, RC, Murakami, T. *Materials Research Society Symposium Proceedings* 1994**; 333**: 653.
3. Takano, Y. *American Mineralogist* 1961**; 46**: 812.
4. Ross, M, Evans, HT, Jr. *American Mineralogist* 1964**; 49**: 1578.
5. Ross, M. *American Mineralogist* 1963**; 48**: 1389.
6. Hanic, F. *Czechoslovak Journal of Physics* 1960**; 10**: 169.
7. Cejka, J, Urbanec, Z, Cejka, J, Jr., Ederova, J, Muck, A. *Journal of Thermal Analysis* 1988**; 33**: 395.
8. Ambartsumyan, TL. *Atomnaya Energ., Voprosy Geol. Urana, Suppl.* 1957: 86.
9. Cejka, J, Cejka, J, Jr., Muck, A. *Thermochimica Acta* 1985**; 86**: 387.
10. Muto, T. *Mineralogical Journal* 1965**; 4**: 245.
11. Locock, AJ, Burns, PC. *American Mineralogist* 2003**; 88**: 240.
12. Cejka, J, Jr., Muck, A, Cejka, J. *Physics and Chemistry of Minerals* 1984**; 11**: 172.
13. Zolensky, ME. *The structures and crystal chemistry of the autunite and meta-autunite mineral groups* 1983.
14. Burns, PC, Miller, ML, Ewing, RC. *Canadian Mineralogist* 1996**; 34**: 845.
15. Miller, SA, Taylor, JC. *Zeitschrift fuer Kristallographie* 1986**; 177**: 247.
16. Martens, W, Frost, RL, Williams, PA. *Journal of Raman Spectroscopy* 2003**; 34**: 104.
17. Martens, WN, Frost, RL, Kloprogge, JT, Williams, PA. *American Mineralogist* 2003**; 88**: 501.
18. Frost, RL, Kloprogge, T, Weier, ML, Martens, WN, Ding, Z, Edwards, HGH. *Spectrochimica Acta, Part A: Molecular and Biomolecular Spectroscopy* 2003**; 59**: 2241.
19. Frost, RL, Weier, ML, Martens, W, Kloprogge, JT, Ding, Z. *Thermochimica Acta* 2003**; 403**: 237.
20. Frost, RL, Weier, ML. *Thermochimica Acta* 2003**; 406**: 221.
21. Frost, RL, Weier, ML, Kloprogge, JT. *Journal of Raman Spectroscopy* 2003**; 34**: 760.
22. Frost, RL, Weier, ML. *Journal of Raman Spectroscopy* 2003**; 34**: 776.
23. Frost, RL, Weier, ML. *Thermochimica Acta* 2004**; 409**: 79.
24. Cejka, J, Jr., Muck, A, Cejka, J. *Neues Jahrbuch fuer Mineralogie, Monatshefte* 1985: 115.
25. Cejka, J. *Reviews in mineralogy* 1999**; 38**.
26. Gevork'yan, SV, Povarennykh, AS. *Mineralogicheskii Zhurnal* 1980**; 2**: 29.
27. Muck, A, Cejka, J, Jr., Cejka, J, Urbanec, Z. *Sbornik Vysoke Skoly Chemicko-Technologicke v Praze, B: Anorganicka Chemie a Technologie* 1986**; B 31**: 71.
28. Omori, K, Seki, T. *Ganseki Kobutsu Kosho Gakkaishi* 1960**; 44**: 7.
29. Urbanec, Z, Cejka, J. *Casopis Narodniho Muzea v Praze, Rada Prirodovedna* 1979**; 148**: 16.
30. Nikanovich, MV, Kovrikov, AB, Popov, VG, Sevchenko, AN, Umreiko, DS. *Doklady Akademii Nauk SSSR* 1976**; 231**: 320.
31. Prins, G. Uranyl chloride, its hydrates, and basic salts; React. Centrum Nederland,Petten,Neth., 1973; pp. 115 pp.

32. Prins, G, Cordfunke, EHP. *Journal of Inorganic and Nuclear Chemistry* 1975**; 37**: 119.
33. Bagnall, KW, Wakerley, MW. *Journal of Inorganic and Nuclear Chemistry* 1975**; 37**: 329.
34. Biwer, BM, Ebert, WL, Bates, JK. *Journal of Nuclear Materials* 1990**; 175**: 188.
35. Bukalov, SS, Vdovenko, VM, Ladygin, IN, Suglobov, DN. *Zhurnal Prikladnoi Spektroskopii* 1970**; 12**: 341.
36. Bullock, JI. *Journal of the Chemical Society [Section] A: Inorganic, Physical, Theoretical* 1969**; 5**: 781.
37. Maya, L, Begun, GM. *Journal of Inorganic and Nuclear Chemistry* 1981**; 43**: 2827.
38. Frost, RL, Martens, WN, Kloprogge, T, Williams, PA. *Neues Jahrbuch fuer Mineralogie, Monatshefte* 2002: 481.
39. Frost, RL, Williams, PA, Martens, W, Kloprogge, JT, Leverett, P. *Journal of Raman Spectroscopy* 2002**; 33**: 260.
40. Farmer, VC *Mineralogical Society Monograph 4: The Infrared Spectra of Minerals*, 1974.

Table 1 Raman spectroscopic analysis of saléeite at elevated temperatures

	30 °C	40 °C	55 °C	75 °C	100 °C	150 °C	250 °C
Band centre/cm^{-1}	3615	3615	3614	3614	3612	3612	
Bandwidth/cm^{-1}	18.7	38.6	16.1	17.0	21.8	24.4	
Relative Intensity/%	25.0	23.9	31.5	42.2	34.0	100	
Band centre/cm^{-1}	3536	3533	3602	3581			
Bandwidth/cm^{-1}	42.6	54.4	38.5	74.4			
Relative Intensity/%	44.1	62.7	21.4	49.8			
Band centre/cm^{-1}	3496						
Bandwidth/cm^{-1}	30.4						
Relative Intensity/%	4.0						
Band centre/cm^{-1}	3400	3391	3400				
Bandwidth/cm^{-1}	74.4	75.1	121.5				
Relative Intensity/%	26.9	13.4	47.0				
Band centre/cm^{-1}				3376	3344		
Bandwidth/cm^{-1}				49.0	188.0		
Relative Intensity/%				8.0	66.0		
Band centre/cm^{-1}	1007	1008					1036
Bandwidth/cm^{-1}	11.8	14.2					54.7
Relative Intensity/%	10.0	20.6					12.8
Band centre/cm^{-1}	994	994	995	995	995	994	997
Bandwidth/cm^{-1}	12.8	11.1	15.5	13.0	14.5	16.3	20.3
Relative Intensity/%	22.7	13.5	34.8	35.1	29.3	29.8	18.0
Band centre/cm^{-1}	980	978	977	977	978	979	
Bandwidth/cm^{-1}	13.1	11.7	10.6	10.6	10.8	11.5	
Relative Intensity/%	21.7	23.1	8.1	9.2	6.6	10.9	
Band centre/cm^{-1}			927	926	927	927	934
Bandwidth/cm^{-1}			7.0	7.8	8.8	10.9	26.0
Relative Intensity/%			0.67	0.95	2.1	2.5	3.3
Band centre/cm^{-1}	894	891					
Bandwidth/cm^{-1}	4.4	13.6					
Relative Intensity/%	0.14	0.47					
Band centre/cm^{-1}	843	841	843	843	843	842	
Bandwidth/cm^{-1}	10.6	12.6	8.2	7.7	7.9	8.4	
Relative Intensity/%	15.1	14.3	43.0	45.9	42.7	28.9	
Band centre/cm^{-1}	827	825	826	827	839	838	829
Bandwidth/cm^{-1}	13.7	11.0	15.0	13.9	26.8	21.9	22.1

Relative Intensity/%	18.5	18.1	8.4	5.4	19.4	28.0	65.9
Band centre/cm^{-1}	803	801	811	812			
Bandwidth/cm^{-1}	17.6	20.5	26.7	24.1			
Relative Intensity/%	11.7	9.8	4.8	3.3			
Band centre/cm^{-1}	612	613	609	609	609	608	612
Bandwidth/cm^{-1}	14.0	15.0	9.2	8.6	9.1	9.6	22.1
Relative Intensity/%	13.0	10.6	12.5	13.4	13.2	13.8	16.3
Band centre/cm^{-1}	573	573		582	581	577	575
Bandwidth/cm^{-1}	28.7	29.9		13.7	18.5	54.4	26.4
Relative Intensity/%	6.5	9.5		0.8	1.76	3.2	3.5
Band centre/cm^{-1}	471	471	471	472	470	470	468
Bandwidth/cm^{-1}	17.4	17.2	14.6	14.0	15.9	17.0	26.0
Relative Intensity/%	11.7	7.7	28.9	30.8	37.4	36.5	38.0
Band centre/cm^{-1}	446	445	451	451			
Bandwidth/cm^{-1}	16.8	15.9	25.2	24.9			
Relative Intensity/%	11.1	21.8	6.1	5.7			
Band centre/cm^{-1}	405	405	405				
Bandwidth/cm^{-1}	9.4	11.0	10.3				
Relative Intensity/%	5.6	9.5	1.0				
Band centre/cm^{-1}	376	377	371	370	370	371	
Bandwidth/cm^{-1}	23.9	24.9	12.0	9.3	11.4	11.3	
Relative Intensity/%	3.0	3.76	2.7	2.3	3.86	2.7	
Band centre/cm^{-1}	283	284	282	283	283	281	272
Bandwidth/cm^{-1}	20.4	17.9	21.0	15.8	17.4	18.4	27.0
Relative Intensity/%	34.6	27.6	34.4	27.2	25.0	28.0	19.0
Band centre/cm^{-1}				265	266	264	268
Bandwidth/cm^{-1}				18.7	18.2	13.9	25.0
Relative Intensity/%				7.7	5.1	3.8	20.9
Band centre/cm^{-1}	234	234	235	236	235	235	
Bandwidth/cm^{-1}	10.1	10.1	9.1	9.6	9.9	10.6	
Relative Intensity/%	3.4	2.15	8.8	6.7	6.23	6.4	
Band centre/cm^{-1}	218	217	216	214	213	213	
Bandwidth/cm^{-1}	12.0	11.0	9.6	8.7	8.8	9.7	
Relative Intensity/%	4.6	2.2	4.2	3.5	5.2	2.3	
Band centre/cm^{-1}	196	196	197	196	197	200	197
Bandwidth/cm^{-1}	11.4	10.8	7.0	6.9	5.5	12.5	8.4
Relative Intensity/%	6.0	5.0	1.8	0.78	0.9	2.1	2.1

Band centre/cm^{-1}	177	177			182	179	177
Bandwidth/cm^{-1}	8.1	5.0			5.4	9.9	6.8
Relative Intensity/%	0.65	0.16			1.16	0.9	0.8

LIST OF FIGURES

LIST OF TABLES

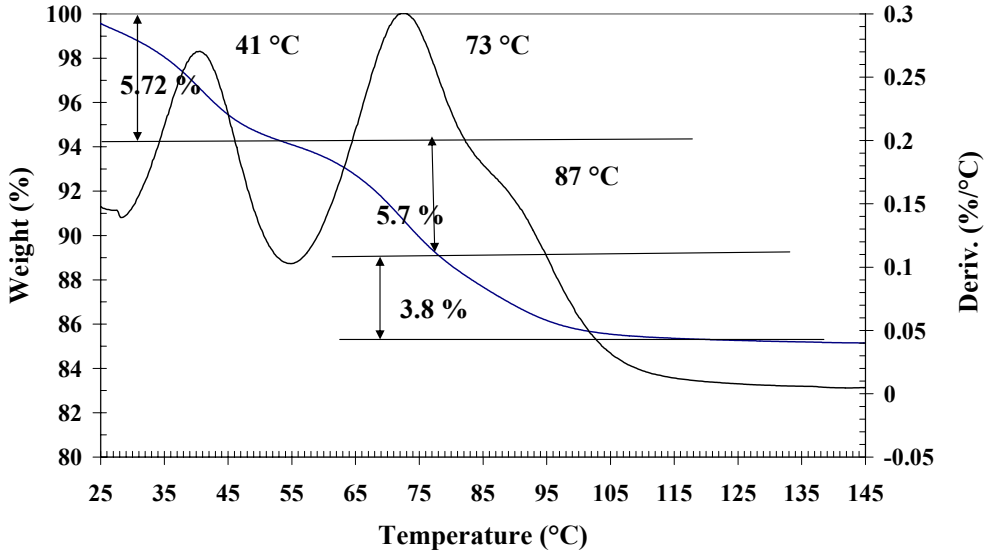

Figure 1a

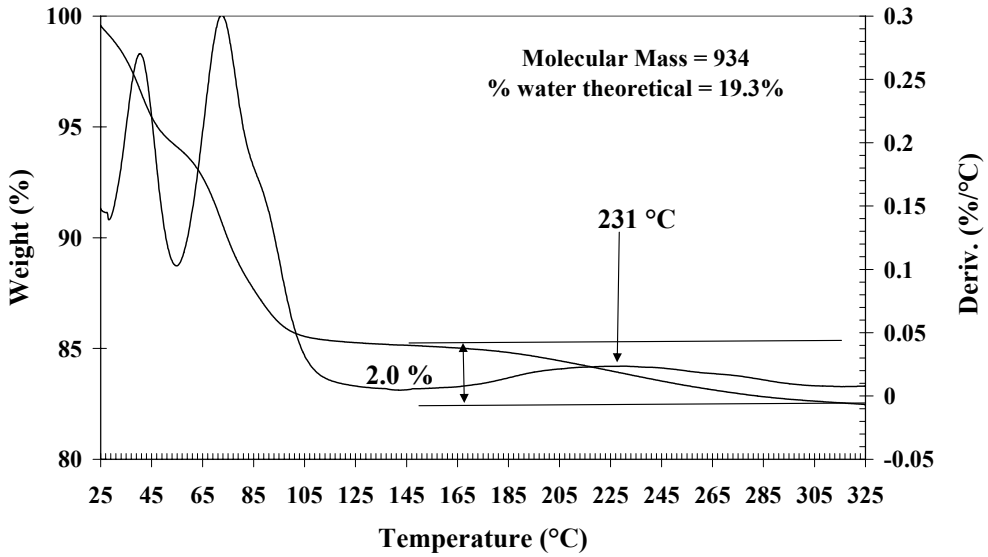

Figure 1b

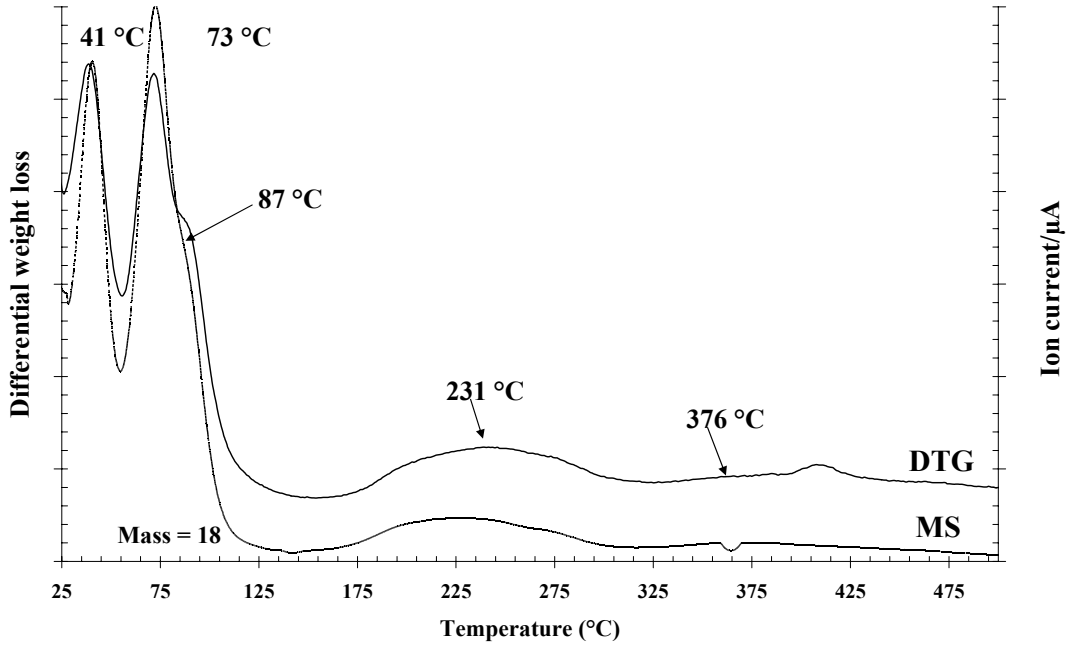
41 °C
73 °C
87 °C
231 °C
376 °C
DTG
MS
Mass = 18
Differential weight loss
Ion current/µA
25
75
125
175
225
275
325
375
425
475
Temperature (°C)

Figure 2

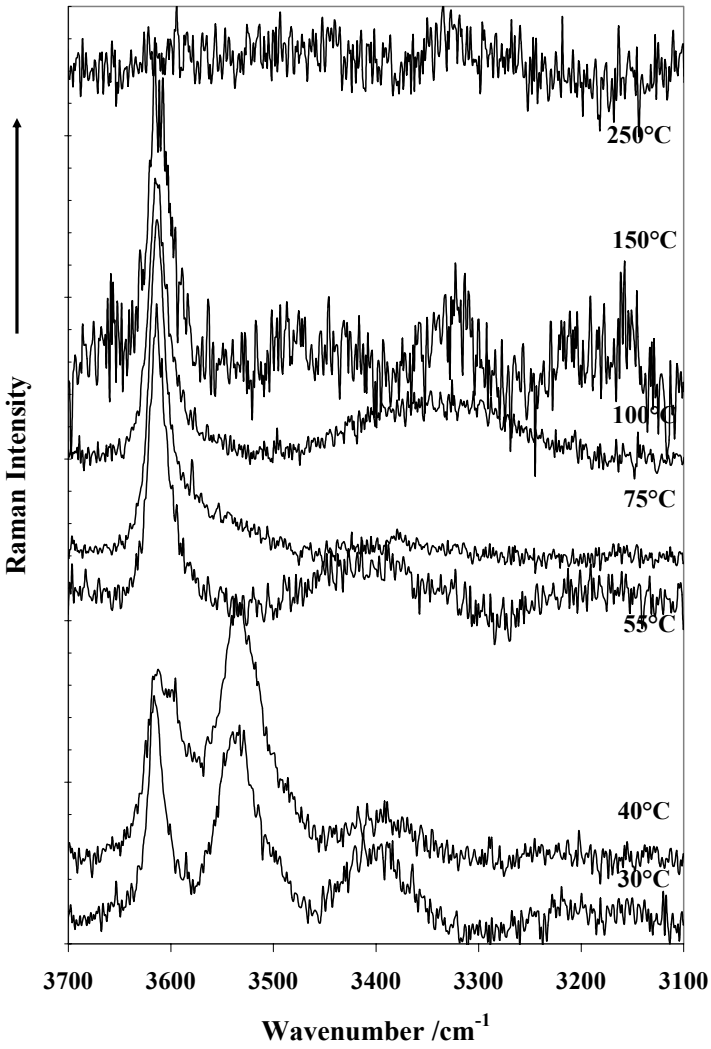
Raman Intensity
250°C
150°C
100°C
75°C
55°C
40°C
30°C
3700
3600
3500
3400
3300
3200
3100
Wavenumber /cm-1

Figure 3

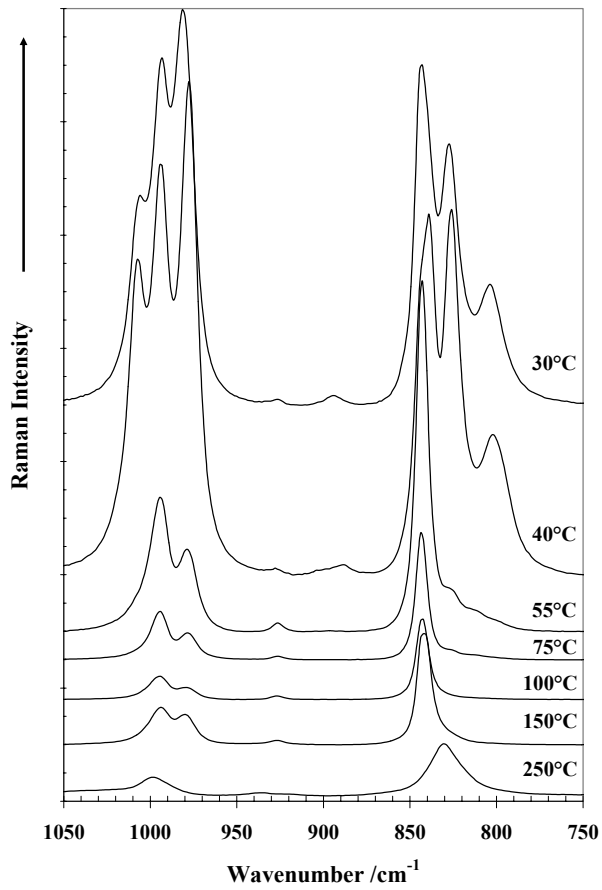
Raman Intensity
30°C
40°C
55°C
75°C
100°C
150°C
250°C
1050
1000
950
900
850
800
750
Wavenumber /cm-1

Figure 4

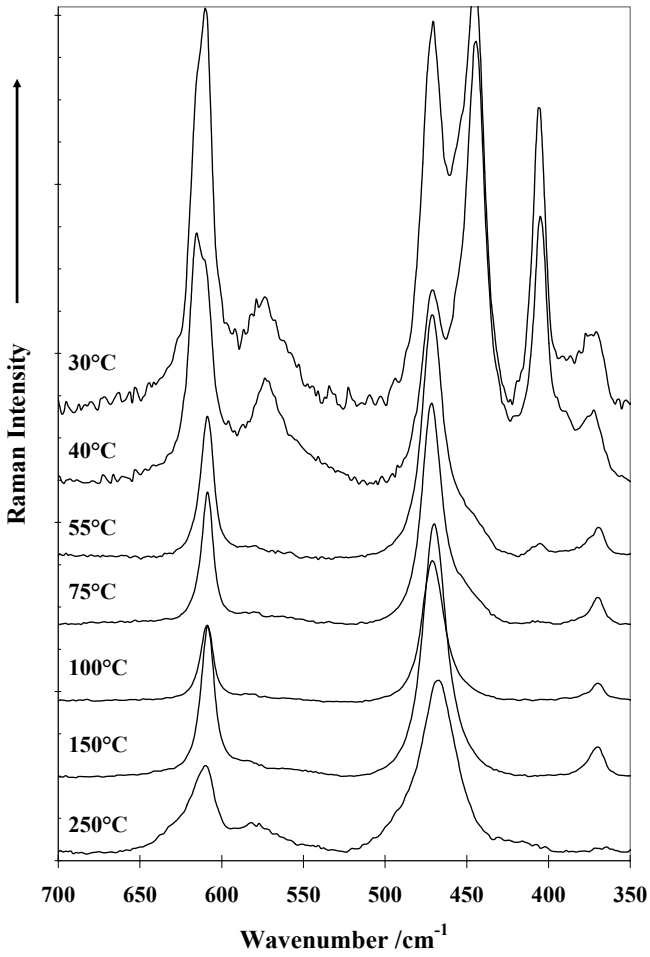
Raman Intensity
30°C
40°C
55°C
75°C
100°C
150°C
250°C
700
650
600
550
500
450
400
350
Wavenumber /cm-1

Figure 5

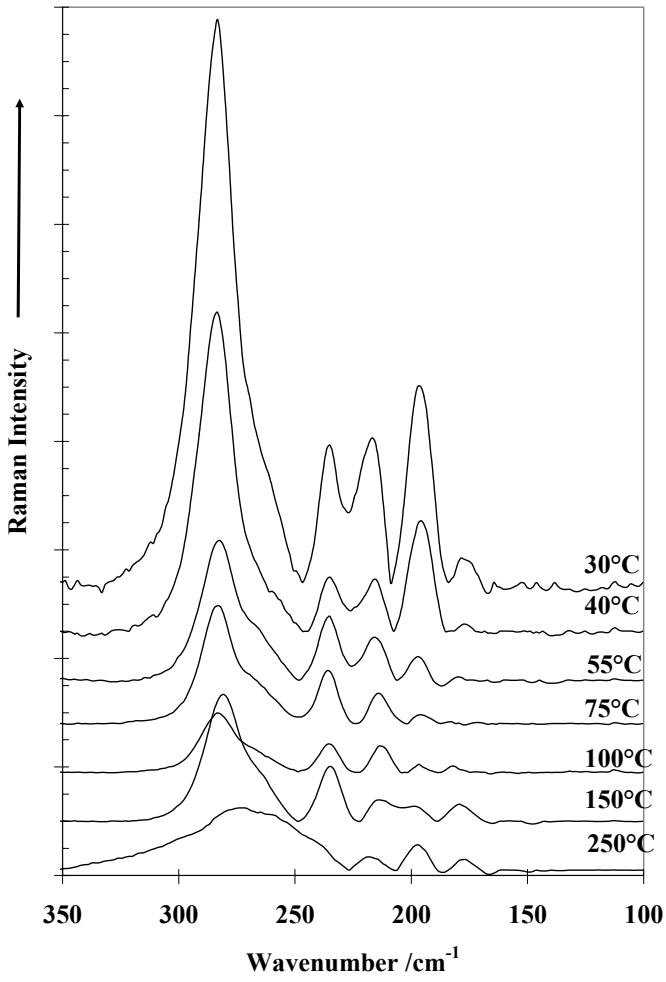
Raman Intensity
30°C
40°C
55°C
75°C
100°C
150°C
250°C
350
300
250
200
150
100
Wavenumber /cm-1

Figure 6